- X-ray created warm dense matter and plasma traced with Boltzmann kinetic equations -

Application of Boltzmann kinetic equations to model X-ray created warm dense matter and plasma

Beata Ziaja (1,2,*), John Jasper Bekx (1), Martin Masek (3), Nikita Medvedev (3,4),

Vladimir Lipp (2,1), Vikrant Saxena (1,5), Michal Stransky (6,3)

(1) Center for Free-Electron Science CFEL, Deutsches Elektronen-Synchrotron DESY, Notkestr. 85, 22607 Hamburg, Germany

(2) Institute of Nuclear Physics, Polish Academy of Sciences, Radzikowskiego 152, 31-342 Krakow, Poland

(3) Institute of Physics, Czech Academy of Sciences, Na Slovance 2, 182 21 Prague 8, Czech Republic

(4) Institute of Plasma Physics, Czech Academy of Sciences, Za Slovankou 3, 182 00 Prague 8, Czech Republic

(5) Department of Physics, Indian Institute of Technology Delhi, New Delhi 110016, India

(6) European XFEL, Holzkoppel 4, 22869 Schenefeld, Germany

(*) Corresponding author: ziaja@mail.desy.de

Abstract: In this review, we describe application of Boltzmann kinetic equations for modeling warm dense matter and plasma formed after irradiation of solid materials with intense femtosecond X-ray pulses. Classical Boltzmann kinetic equations are derived from the reduced N-particle Liouville equations. They include only single-particle densities of ions and free electrons present in the sample. The first version of the Boltzmann kinetic equation solver was completed in 2006. It could model non-equilibrium evolution of X-ray irradiated finite-size atomic systems. In 2016, the code was adapted to study plasma created from X-ray irradiated materials. Additional extension of the code was then also performed, enabling simulations in hard X-ray irradiation regime. In order to avoid treatment of very high number of active atomic configurations involved in the excitation and relaxation of X-ray irradiated materials, an approach called “predominant excitation and relaxation path” was introduced. It limited the number of active atomic configurations by following the sample evolution only along the most probable excitation and relaxation paths. The performance of the Boltzmann code is illustrated on the examples of X-ray heated solid carbon and gold. Actual model limitations and further model developments are discussed.

- X-ray created warm dense matter and plasma traced with Boltzmann kinetic equations -

1. Introduction

Already for two decades the X-ray free-electron lasers (XFELs), e.g., **[Acker07,Alla12,Emma10, Pile11,Weis17]**, enable a unique insight into previously unavailable and still not fully explored regime of ultrafast processes occurring in matter on femtosecond timescales. Intense X-ray pulses from XFELs may serve as a probe, providing access to the information on transient electronic and structural transitions in matter, acquired, among others, with the powerful technique of coherent diffraction imaging. The X rays may also act as a pump, triggering strong excitation of electronic subsystem on femtosecond timescales. This brings the matter into an extreme regime, see, e.g., **[Gorkh14,Tachi15,Inou21]**, in particular into the transient warm-dense-matter (WDM) regime **[Vink12,Zastr14,Levy15].** WDM is the state of matter at the frontier between a plasma and a condensed phase. It is key to astrophysics, planetary science and inertial confinement fusion research, but its electronic and ionic structure and dynamics remain poorly understood.

For the analysis of experimental results on X-ray created WDM and plasma, a development of dedicated theoretical tools, able to describe the evolution of these states under strongly non-equilibrium conditions, is necessary Especially, warm dense matter represents a modeling challenge, bordering between plasma state and solid state. Modeling approaches actually use either condensed matter physics tools or plasma physics tools. We will report here on the latter approach, using a plasma simulation tool and atomistic approximation.

We then assume that our sample initially consists of unbound atoms. Appearance of ions and free electrons follows as a result of X-ray irradiation. Modeling of ionization dynamics in such a sample can be efficiently performed, using a continuum approach **[Ethi01,Ziaj06,Sherl13]**. Such an approach solves evolution equations on phase-space grid for density distributions of electrons, atoms and ions. This significantly reduces computational costs as they depend only on the grid size, and do not scale quadratically with particle number, $O(N^2)$, as typically with particle approaches. This enables to treat efficiently also large samples. The simulation of the non-equilibrium stage of the sample evolution requires application of full kinetic equations, delivering the information on the transient electron and ion distributions and including all atomic configuration active during the excitation and relaxation of the irradiated sample.

Another modeling difficulty is that energetic X rays can release inner-shell electrons, leaving core holes behind. The holes can relax along complex pathways, especially in heavier elements. This relaxation also involves collisional processes and a large number of active atomic configurations. Their very high number can make the respective set of evolution equations (including each configuration) practically insolvable. For example, the total number of atomic configurations in carbon (Z=6) is 27, where Z is the atomic number. The corresponding set of evolution equations can then be easily solved for all the configurations. The same is valid for other light elements. But this is already not the case for

noble gases, neon (Z=10), and argon (X=18), where the total numbers of atomic configurations are 63 and 1323 respectively. The rapid increase of the atomic configuration number as a function of Z limits the application of kinetic simulations to low-Z materials. In order to avoid this problem, a superconfiguration approach, see e.g., **[Chun05],** can be used, which does not treat individual atomic configurations but uses instead a set of 'averaged' configurations **[Lee87,March90]**.

An alternative scheme was proposed in **[Ziaj16].** Therein, in order to avoid the treatment of a very high number of active atomic configurations involved in the excitation and relaxation of the X-ray irradiated materials, an approach called “predominant excitation and relaxation path” (PERP) was introduced. It limited the number of active atomic configurations by following the sample excitation and relaxation only along the most probable relaxation paths (including predominant collisional processes). This will be discussed in detail below.

In what follows, we will first describe the kinetic equation approach for X-ray irradiated samples. Its extension for simulations of irradiated solid materials will then be discussed. The performance of the Boltzmann code will be demonstrated on the example of warm dense matter carbon and gold, the latter in comparison to the available experimental data. Finally, the current model limitations and their possible improvements will be discussed.

2. Kinetic equation approach to model X-ray irradiated samples.

2.1 Physical picture

Our Boltzmann kinetic equations solver, dedicated to describe the evolution of X-ray irradiated samples, was developed and improved in the following papers: **[Ziaj06, Ziaj07, Ziaj08, Ziaj081, Ziaj09, Ziaj091, Faus10, Ziaj11, Ziaj16].** Classical Boltzmann kinetic equations are derived from the reduced N-particle Liouville equations. They follow the evolution of single-particle densities in phase-space. We adapted them to model X-ray irradiated solid or plasma systems, assuming that these samples are built of ions in various atomic configurations and of free electrons (atomistic approximation). Each of these constituents is represented by a classical **phase-space** density. The resulting set of kinetic equations for the electron distribution in phase-space, $\rho^{(e)}$, and for distributions of various atomic configurations, $\rho^{(i,j)}$, is:

$$\partial_t \rho^{(e)}(\mathbf{r},\mathbf{v},t) + \mathbf{v} \cdot \partial_{\mathbf{r}} \rho^{(e)}(\mathbf{r},\mathbf{v},t) - \mathbf{F}_{\mathbf{EM}}(\mathbf{r},\mathbf{v},t)/m \cdot \partial_{\mathbf{v}} \rho^{(e)}(\mathbf{r},\mathbf{v},t) = \Omega^{(e)}(\rho^{(e)},\rho^{(i,j)},\mathbf{r},\mathbf{v},t) \quad (1)$$

for electrons, and:

- X-ray created warm dense matter and plasma traced with Boltzmann kinetic equations -

$$\partial_t \rho^{(i,j)}(\mathbf{r},\mathbf{v},t) + \mathbf{v} \cdot \partial_{\mathbf{r}} \rho^{(i,j)}(\mathbf{r},\mathbf{v},t) + i \cdot \mathbf{F}_{\mathbf{EM}}(\mathbf{r},\mathbf{v},t)/M \cdot \partial_{\mathbf{v}} \rho^{(i,j)}(\mathbf{r},\mathbf{v},t) = \Omega^{(i,j)}(\rho^{(e)},\rho^{(i,j)},\mathbf{r},\mathbf{v},t) \quad (2)$$

for various atomic configurations. The index, $i=0$,.., N_J, denotes the ion charge (with N_J being the highest charge state in the system), and the index, $j=0,..,N_C(i)$, denotes the active configuration number (with $N_C(i)$ being the maximal number of ion configurations considered for a fixed *ith* ion charge). Electron and ion masess are, *m*, and, *M*, respectively.

Generally, there are two components of the electromagnetic force, $\boldsymbol{F}_{EM} = -e \cdot (\boldsymbol{E}(r,t) + \boldsymbol{v} \times \boldsymbol{B}(r,t))$ in Eq. (1) (similarly for ions, Eq.(2)): the electric one, $-\boldsymbol{e} \cdot \boldsymbol{E}(r,t)$ and the magnetic one, $-\boldsymbol{e} \cdot (\boldsymbol{v} \times \boldsymbol{B}(r,t))$. The symbol *e* denotes here the magnitude of electron charge. The electromagnetic force describes the interaction between the charges in the sample and the external laser field and the mutual interactions between the charges. However, magnetic component of the electromagnetic interaction, $\boldsymbol{B}(r,t)$, as well as the interaction of the laser field, $\boldsymbol{E}(r,t)$, with charged particles in the sample can be neglected in case of X-ray irradiation (for more details, see **[Ziaj06])**. This reduces the force to the component representing electrostatic interactions between charges in the sample - a non-local function of electron and ion densities. It was formulated in **[Ziaj06]** (see Eq. (5) therein).

Initial conditions for Eqs. (1-2) are given by a neutral atom distribution function. The free electron distribution is equal to zero. During the non-equilibrium evolution of X-ray irradiated samples, the emerging free-electron and ion densities change: (i) due to photoinduced processes such as photoexcitation and Auger decay, and (ii) due to the electronic collisional processes including elastic electron-ion collision, electron impact ionization and three-body recombination. These effects are modeled with the collision terms, $\Omega^{(e)}$ and $\Omega^{(i,j)}$. They describe the respective changes of transient electron and ion densities due to the above processes and also due to the short range electron-electron scattering **[Shar66]**. The respective rates and cross sections are derived in the atomistic approximation, i.e., assuming the interaction of an isolated atom with an impact particle. They are included into two and three body Boltzmann collision integrals in the equations (for details see, e.g. **[Aris01,Shar66]**). The rates and cross sections of atomic processes induced by X-ray photons were calculated with the XATOM code **[Son11,Jur16]**. The collisional ionization cross sections (and the respective recombination rates were obtained from the Lotz formulas **[Lotz70]**. The short range electron-electron scattering was modeled, using the Fokker-Planck collision integral **[Shar66]**. As the electron system is treated as a classical one in this model, the Pauli blocking effect is not included. More details can be found in Ref. **[Ziaj06]**. Please note that if the collision terms are put equal to zero, the Boltzmann equations, Eqs. (1-2), reduce to the Vlasov equations **[Shar66]** which follow the evolution of a collisionless plasma.

The terms on the left-hand-side and right-hand-side of the equations, Eq. (1-2), *per construction* conserve the particle number and the total energy in the system. This applies also for the numerical

algorithms applied to solve the kinetic equations **[Ziaj06]**. It was checked by dedicated tests in all numerical implementations of the Boltzmann equations performed so far.

The first version of the Boltzmann equation solver was described in **[Ziaj06]** and applied there to study noble-gas clusters irradiated with VUV/XUV radiation. Kinetic equations applied included only ground-state ion configurations because the incoming XUV photons could excite electrons only from valence levels. The inverse bremsstrahlung process contributed to the free electron heating in this photon energy regime. As femtosecond timescales were there considered, the electron recombination could be neglected. Further code applications to noble gas systems followed, with ionic time-of-flight spectra studied there. They were presented in Refs. **[Ziaj07,Ziaj08,Ziaj081]**.

In **[Ziaj09],** the modeling of three-body recombination was added to the code, extending its applicability. In **[Ziaj091],** the analysis of the electron spectra was for the first time performed with the Boltzmann equations, without any 'instantaneous thermalization' assumption, frequently applied at that time (see, e.g. **[Hau12]).** The first application of the code to model non-equilibrium finite-size WDM and plasma was performed in **[Faus10].** Femtosecond thermalization of electrons created after X-ray irradiation of hydrogen was studied there. Also heterogeneous samples, consisting of different elements, were studied with the Boltzmann code. In **[Ziaj11],** for the first time atomic clusters containing atoms of two noble gases, could be successfully treated.

Later, in **[Ziaj16]**, the Boltzmann equation solver was modified to enable studies of warm dense matter and plasma created from bulk materials irradiated by X rays. High-intensity X-ray pulses can trigger spatially homogeneous ionization dynamics within a large volume inside the irradiated material. The necessary conditions are: wide beam focusing and the thickness of the target layer comparable to the penetration depth of the X-ray photons **[Vink15]**. The homogeneous ionization dynamics implies that both electron and ion distributions can be assumed to be spatially uniform. Their evolution then becomes **r**-independent:

$$\partial_{\mathbf{r}}\rho^{(e)}(\mathbf{r},\mathbf{v},t) = 0$$
$$\partial_{\mathbf{r}}\rho^{(i,j)}(\mathbf{r},\mathbf{v},t) = 0 \qquad (3)$$

The direct consequence of the spatial charge homogeneity is the quasineutrality within the sample: at each space point the electron and gross ion charges are identical. This makes the component of the electrostatic force representing mutual interactions of electrons and ions equal to zero. The modified equations still treat fast electron thermalization, as the short-range electron-electron interaction term is unaffected by Eq. (3).

Numerical solving of Boltzmann equations is significantly faster with these simplifications, when comparing to the case of finite samples, as no adaptive stability condition is then needed. This enables computationally efficient simulations of ionization dynamics within X-ray irradiated bulk material. For more details, see **[Ziaj16]**.

Another extension of the code was performed, enabling treatment of hard X-ray irradiation. In order to avoid the bottleneck of very high number of active atomic configurations involved in the excitation and relaxation of X-ray irradiated materials, an approach called "predominant excitation and relaxation path" (PERP) was introduced in **[Ziaj16]**. It limited the number of active atomic configurations by following the sample relaxation along the most probable relaxation paths (including also collisional relaxation processes). Their choice was determined by the largest cross sections and transitions rates. For example, the simplest PERP scheme includes only atomic configurations present in the excitation and relaxation paths with the most probable photoionization processes and the most probable Auger decays, and the predominant collisional ionization processes (from/to the valence shell of all considered atoms and ions). The accuracy of the scheme was tested in **[Ziaj16]** for carbon by performing PERP calculations and comparing them to the results obtained with a calculation including all relaxation paths. Further successful benchmarking, using a molecular dynamics code**,** was made later **[Abd17]**.

The choice of the predominant excitation and relaxation paths for an X-ray irradiated material is now performed automatically at the specified pulse conditions by a dedicated script - before the simulation starts. The script allows to apply the approach also to heavy elements (after including radiative decays of core holes), and practically at all X-ray photon energies, available at the currently operating XFEL facilities (< 30 keV).

2.2 Numerical implementation

Equations **(1), (2)** are integro-differential equations, in the most general case, in six-dimensional phase space. Therefore, only their numerical solution is possible. A significant simplification of the kinetic equations can be achieved: (i) if considering samples with a symmetry, and (ii) if applying the angular moment expansion for the electron and ion densities **[Pons99,Shar66,Kruer88]**. In the latter case, the isotropic components of the electron and ion phase-space density distributions should be predominant. This implies, in particular, that the velocity component of collective transport has to be small. If applying in addition the condition, Eq. (3), this reduces the number of dimensions ultimately to one (the magnitude of the velocity, $|\mathbf{v}|$).

The spatially uniform Boltzmann equations for a bulk material are then solved on a grid in velocity space, applying dedicated numerical methods **[Press03,Boyd00,Gott77]**. The pseudospectral

method **[Gott77]** is used to efficiently evaluate integrals and partial derivatives in Boltzmann equations. The solver has been carefully tested to check its numerical accuracy. As mentioned earlier, it is conservative in respect to the particle number and total energy, if the source terms are set equal to zero **[Ziaj06].** The code is computationally efficient and can be parallelized. At typical XFEL parameters, a run on a single CPU core takes between a few hours and a few days.

3. Performance of kinetic Boltzmann equations model for X-ray heated carbon and gold.

In **[Ziaj16]**, we tested the PERP concept for a light element, carbon (Z=6). Carbon bulk of diamond density was irradiated there with: (i) a soft X-ray pulse of E_{photon}=1000 eV and of maximal intensity of 10^{16}W/cm^2, and (ii) hard X ray pulse of E_{photon}=5000 eV and maximal intensity of 10^{18}W/cm^2. Using our Boltzmann solver, we checked that both the average charge and average energy absorbed per atom predicted with full calculation (including all 27 atomic configurations) and with the PERP scheme were in a good agreement.

In **[Ziaj21],** we applied our code to a heavy element, gold (Z=79). It was chosen because many theoretical and experimental data from the warm dense matter regime of gold exist (see, e.g., **[Ng16]**). The adapted code (with the PERP approach inside) could treat charges up to +9, including 144 various ion configurations of Au. The number of photoinduced transitions between those configurations was 140. For the study, we applied a set of pulse parameters available at the FLASH experimental facility **[Acker07]** for high-energy-density experiments (photon energy of 245 eV and the FWHM pulse duration of 60 fs). The X-ray pulse irradiated a 30 nm thick layer of Au. The thickness of the Au layer is similar to the attenuation length of 245 eV photons in gold (~37 nm). This prevents the creation of strong gradients for X-ray energy absorbed within the layer. Pulse energy yielded the deposited dose typical for WDM experiments, i.e., 1- 2 MJ/kg.

The 245 eV X-ray photons predominantly excited 4f-shell electrons. The 4f holes left had a lifetime of ~ 6.6 fs. They were filled with electrons, mostly from 5d shell, and 5d Auger electrons were then emitted. Further photoionization of the 4f core hole state to a double core hole state was also occurring. In parallel to photoinduced transitions, the collisional processes induced by released electrons began to contribute to the ionization dynamics as well. This rapidly increased the average ion charge and led to a fast energy redistribution within the electronic system. A local thermodynamic equilibration of electronic system followed on tens of femtoseconds timescale.

For the above specifed X-ray pulse conditions, the Boltzmann kinetic equations model predicted an occurrence of atomic ions of charges up to +4. The ground state configuration (with delocalized 6s electrons) was built from Au+1 ions. Within the PERP approximation, the number of

active configuration for Au +2 ions was 2, and for Au +3 and Au +4 ions was 3. Eight photoinduced transitions were involved.

Fig. 1 shows the average ionization degree of the bulk gold (per atom) (**Fig.1a**) and the relative charge content, i.e., the number of specific Au ions divided by the initial total number of Au atoms (**Fig.1b**), both as a function of time, predicted for the deposited dose of 1.2 MJ/kg. Please recall that in the framework of our atomistic model the 'neutral' bulk contains only ions, Au +1. They are not used for the calculation of <Z>. The predictions are shown on timescales when ionization process is rapid (up to 200 fs after the maximum intensity of FEL pulse (i.e., time zero)).

Fig. 1 Average charge per atom (a) and relative ion content (b) in X-ray irradiated Au layer as a function of time. The deposited X-ray dose was 1.2 MJ/kg. Temporal pulse profile is depicted as well (light blue curve)

(a) (b)

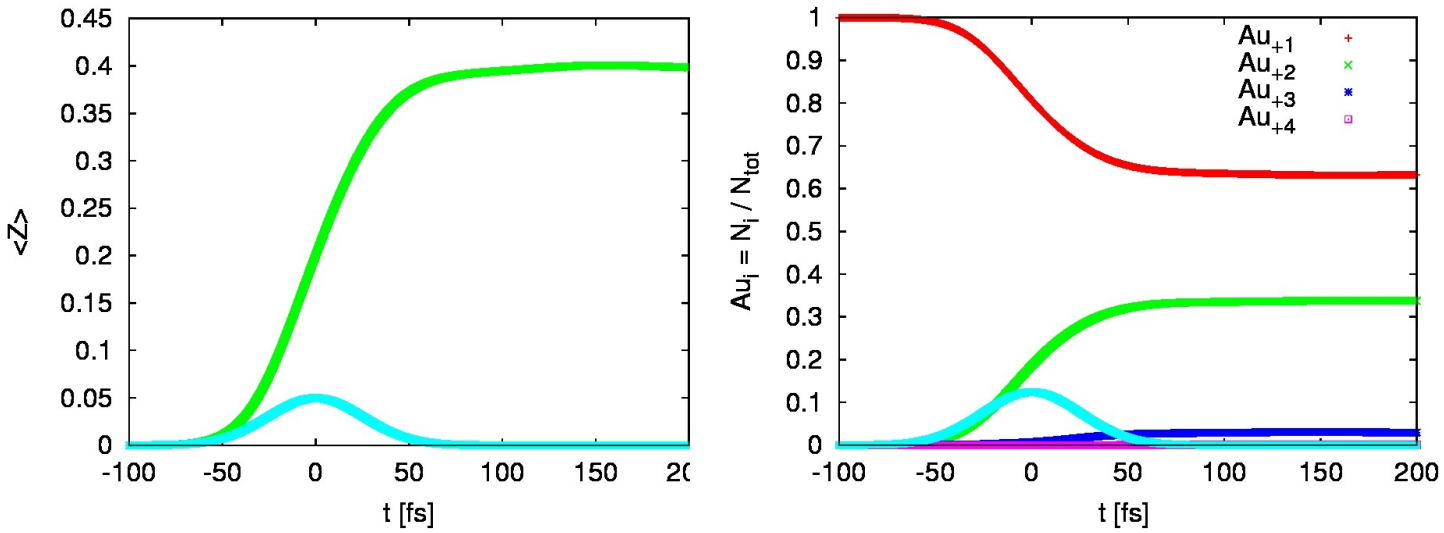

The average charge <Z> per atom strongly grows after the exposure start (**Fig. 1a**). It almost stops to change at ~100 fs, and increases later only slightly. The latter effect is due to the long-timescale Auger decays. Also, three body recombination starts to play a role at later times, increasing the complexity of the relaxation dynamics. The relative ion content can be seen in **Fig. 1b**. It is the largest for Au +1 ions (with one delocalized 6s electron) forming neutral bulk Au. The Au +2 charge states are formed from Au +1 as a result of a core hole excitation 4f or 5p, or after a photo- or impact ionization from level 5d. The ions Au +3 are only a small fraction of the overall number of ions. They can be created through

the Auger decay of a core hole (here 4f → 5d 5d), or through a photoionization or an impact ionization of an Au +2 ion. Creation of Au +4 ions follows a similar pathway.

Fig. 2 show the predicted kinetic electron temperature and transient electron-ion collision time, the latter calculated self-consistently, using the actual electron-ion collision rates, and the transient electron and ion distributions in the sample. The kinetic electron temperature is calculated as 2/3 of the total kinetic energy of all free electrons above the 6s level (calculated with respect to the 6s level) divided by the number of free electrons above the 6s level. After the electron thermalize, the kinetic temperature becomes the Maxwell-Boltzmann temperature. The contribution from the delocalized 6s electrons to the kinetic temperature is neglected within the framework of this model.

Initially, the kinetic electron temperature equals to the temperature of the emitted photoelectrons (~93 eV) after the excitation of a 4f level (**Fig. 2a**). Fast energy exchange among numerous secondary electrons leads to the fast thermalization of the electron distribution already at ~ 50 fs. It is then, when kinetic temperature almost stops to change. The on-going and then completed thermalization is indicated by the electron-ion collision time predicted. Here, this time is defined as an inverse of the total electron-ion collision rate calculated per one electron. It was derived in the same way as described in the Section 2.3 of **[Chun05]**. This calculation takes into account all free electron - bound electron collisions. Initially, the collision time rapidly increases, mimicking the decrease of the kinetic temperature. It reaches a maximum at around -35 fs. It is the same time at which the kinetic T_{el} reaches its minimum. After the thermalization of free electrons is completed, it saturates at the value of ~1.2 fs. This value is in a very good agreement with the equilibrium temperature value measured in Ref. **[Ng16]** after the relaxation of optically excited Au.

Fig. 2 Kinetic electron temperature (a) and transient electron-ion collision time (b) as a function of time. The deposited dose was 1.2 MJ/kg. The maximum of the FEL pulse intensity is at t=0 fs.

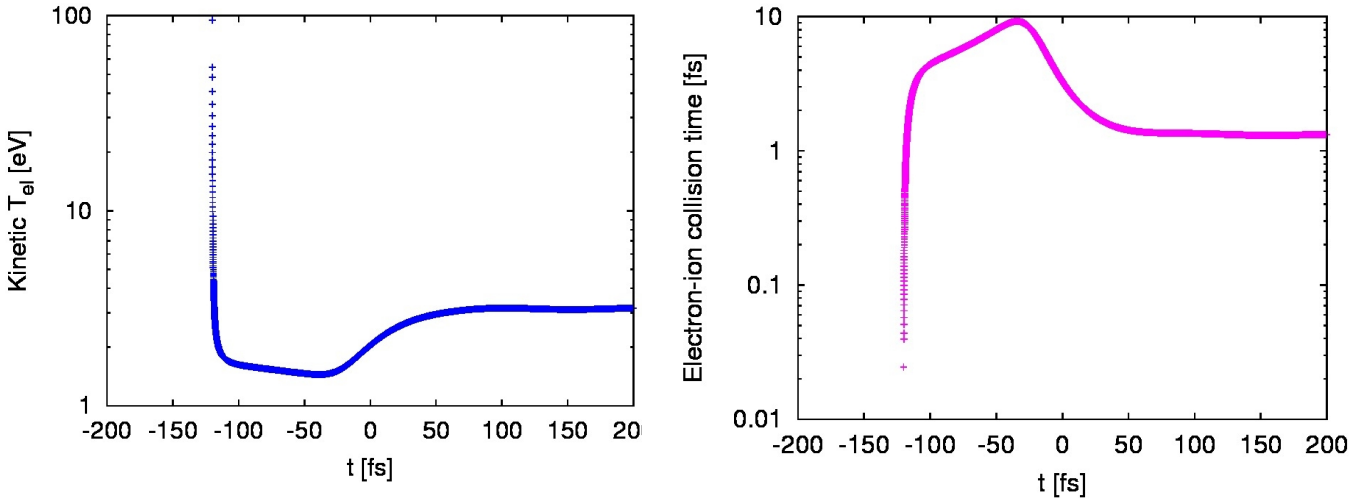

(a) (b)

Fig. 3 shows the transient free-electron-energy distribution, $n_e(E)$ (normalized per electron) as a function of energy. The snapshots are presented for the times: -90 fs, -50 fs, 0 fs (FEL pulse maximum), 50 fs and 90 fs. The normalized free-electron-energy distribution is multiplied by the actual value of the transient ionization degree, <Z>, i.e., the number of free electrons above the 6s level divided by the total number of atoms (**Fig. 1a**), in order to demonstrate the growth of the free electron density per atom in the sample. Each snapshot of the transient electron energy distribution is compared with the corresponding Maxwell-Boltzmann (M-B) distribution obtained using the actual value of kinetic temperature, electron density, and multiplied by the value of the transient ionization degree. Initially, the transient electron energy distributions are distant from the M-B distributions. This occurs both in the low and in the high energy range, where the contribution of photo- and Auger electron peaks to the spectra at ~ 100 eV shows up. After time zero, the latter contribution drops, and the low energy part of the transient spectra approaches the M-B distribution. The M-B curves estimated for times 50 fs and 90 fs are very close to each other, and to the respective transient free-electron-energy distributions. This confirms that the Maxwell-Boltzmann thermalization has been achieved.

Fig. 3 Snapshots of transient electron energy distributions predicted at various time instants (plotted with points), compared to the corresponding Maxwell-Boltzmann distributions (plotted with solid lines of the same color as the points) obtained with the transient values of electron density and kinetic temperature.

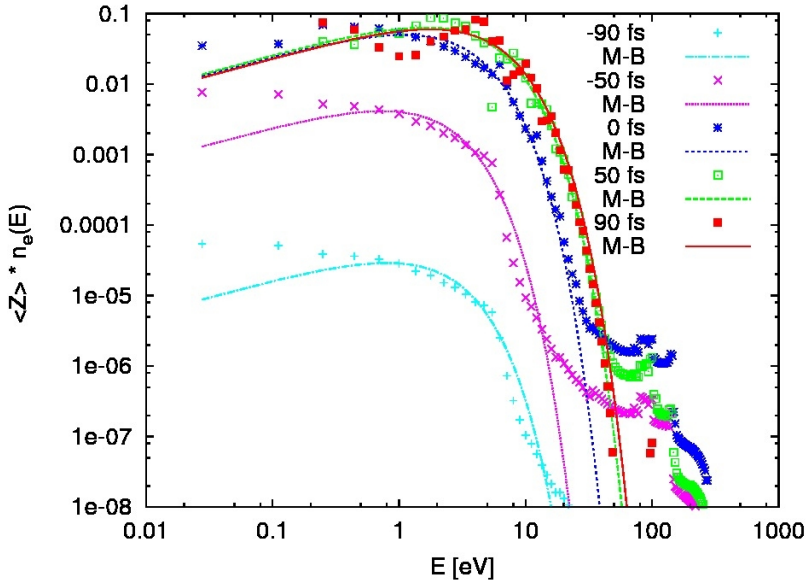

The predictions on free-electron density and electronic temperature can also be used to evaluate the transient optical properties of WDM Au. For example, using Drude model, we calculated the DC conductivity, σ_0, as a function of time, $\sigma_0=\omega_p^2\ \tau\ /\ 4\ \pi$ (not shown). Here, ω_p is the electron plasma frequency, and τ is the electron-ion collision time. The predicted DC conductivity decreases until free electrons thermalize (~ 50 fs) (cf. **Fig. 2**), reaching an equilibrium value of 2.7 x 10^{16} 1/s - in a good agreement with the equilibrium value of ~ 3 x 10^{16} 1/s measured in Ref. **[Ng16]**.

4. Further model developments

4.1 Electron-ion interaction and picosecond evolution times

The Boltzmann equation solver was constructed to describe electron and ion dynamics on maximally a few 100 fs timescale. Due to the large ion-mass-to-electron-mass ratio, the ion recoil during collisions between electron and ions could be neglected. The ions remained 'cold' during the entire simulation.

However, the electron-ion energy exchange and the mutual thermalization of the electron and ion systems have to be treated, when moving to picosecond simulation timescales. Therefore, the original Boltzmann equation solver had to be extended for the electron-ion coupling. Here, it was approximated with the Spitzer rate **[Shar66].** In bulk Au the electron-ion coupling is weak, therefore, it did not much affected the sample evolution on picosecond timescales. The description of the electron-ion coupling can be further improved, using the rates from, e.g., **[Medv20]**. The extended code can then be used for picosecond timescale simulations.

It should be also emphasized that the atomistic plasma code per construction cannot treat band structure. The sample is defined as an ensemble of unbound atoms in this approximation. The interaction of the atoms with X-ray photons and secondary electrons is modeled with atomistic cross sections and rates. This feature cannot be easily improved, besides including bond energy in the simulations.

4.2 Ionization potential lowering

When a solid sample is irradiated with high intensity X-ray pulse, numerous electrons and ions are produced. The ions within the dense plasma formed cannot be any longer modeled as isolated particles due to the plasma environment. For the description of the dense plasma effect on the ionization potential (IP) of the plasma-embedded ions, dedicated modeling **[Mur98]** is required. For the Boltzmann code, the IP lowering can be estimated with the code XATOM for plasmas of various electron densities and temperatures **[Son14, Jur16].** However, the code is prepared for any implementation of the ionization potential shift, either obtained from phenomenological parametrizations **[Mur98]** or from ab-initio approaches, e.g., **[Son14]**. The value of the shift can be changed on-the-fly, as a function of actual plasma parameters.

4.3 Impact ionization cross sections.

In order to include only predominant processes during sample excitation and relaxation, we consistently treated in the code only the predominant collisional ionization processes, i.e., collisional ionization and recombination from/to the outermost shell of all considered atoms and ions. The latter assumption holds for impact electrons of energy less than 1000 eV. However, at higher impact electron energies, collisional core hole excitations become increasingly probable. They have to be taken into account, when extending the application of the Boltzmann code to X-ray irradiation regime with photons of a few keV up to several keV energies. This is planned as future code development.

4.4. Fermi-Dirac statistics.

Boltzmann kinetic equations presented above are classical kinetic equations, with energetic electrons evolving towards Maxwell-Boltzmann distribution. However, one could, in principle, account in the equations also for Pauli blocking **[Reth02,Piet05,Shch13],** after introducing discrete free electron levels. During electron thermalization, this would push electron distribution towards Fermi-Dirac distribution. Such extension of the code is non trivial but feasible. It is also planned as a future development.

5. Conclusions and outlook

We have described the implementation of our Boltzmann kinetic equations solver to simulate warm dense matter and plasma created from bulk systems. It was illustrated in detail on the example of X-ray created warm dense matter gold, also analyzed in **[Ziaj21]**. The Boltzmann model predictions were compared with the available experimental data and found to be in a good agreement with them. This encouraging experience have stimulated further applications of the Boltzmann solver to X-ray heated copper and silicon which are on-going.

With further model developments listed in Section 4, there is a clear prospect for a creation of a comprehensive versatile simulation tool for X-ray irradiated bulk solids, of computational efficiency much higher than that of typical Molecular Dynamics approaches. These projects are underway, and their predictions will undergo validation by dedicated experiments.

Acknowledgements

The authors V.L., N.M., M.S., and B.Z. acknowledge the networking support by the COST Action CA17126.

Author contributions

To simulate bulk materials irradiated with hard X rays, B. Z. modified her kinetic Boltzmann equation solver and used updated material parameters, with contributions of **(i)** N. M. who introduced a subroutine to calculate impact ionization cross sections based on the Lotz approach **[Lotz70]** to the Boltzmann code, and J. J. B. who further improved it, **(ii)** V. L. who introduced a subroutine to calculate elastic electron-ion cross section **[Jenk12]** to the Boltzmann code, and **(iii)** and V. S., M. S., M. M. who contributed to the development of the PERP approach and its automatized implementation. B.Z. wrote the manuscript, with contributions from all authors.

References:

[Abd17] M. M. Abdullah, Anurag, Z. Jurek, S.-K. Son, and R. Santra, *"Molecular-dynamics approach for studying the nonequilibrium behavior of x-ray-heated solid-density matter"*, Phys. Rev. E 96, 023205 (2017).

[Acker07] W. Ackermann, et al., *"Operation of a free-electron laser from the extreme ultraviolet to the water window."*, Nat. Photon. 1 , 336–342 (2007).

[Alla12] E. Allaria, et al., *“Highly coherent and stable pulses from the FERMI seeded free-electron laser in the extreme ultraviolet”*, Nat. Photon. 6 , 699–704 (2012).

[Ashcr76] N. W Ashcroft and N. D. Mermin, in *"Solid state physics"*, Thomson Learning Inc., 1976.

[Aris01] V. V. Aristov, in *"Direct Methods for Solving the Boltzmann Equation and Study of Nonequilibrium Flows"*, Kluwer Academic Publishers, 2001

[Boyd00] J.P. Boyd, in *"Chebyshev and Fourier Spectral Methods"*, Dover Publications Inc., 2000

[Chun05] H.-K. Chung et al., *"FLYCHK: Generalized population kinetics and spectral model for rapid spectroscopic analysis for all elements*", High Energy Density Physics 1, 3- 12 (2005).

[Emma10] P. Emma, et al., *“First lasing and operation of an ångstrom-wavelength free-electron laser.”*, Nat. Photon. 4 , 641–647 (2010).

[Ethi01] S. Ethier and J.P. Matte, *"Electron kinetic simulations of solid density Al plasmas produced by intense subpicosecond laser pulses. I. Ionization dynamics in 30 femtosecond pulses*", Phys. Plasm. 8, 1650 (2001).

[Faus10] R. Fäustlin et al., *"Observation of ultrafast non-equilibrium collective dynamics in a warm dense hydrogen plasma"*, Phys. Rev. Lett 104, 125002 (2010).

[Gorkh14] T. Gorkhover et al., *"Nanoplasma Dynamics of Single Large Xenon Clusters Irradiated with Superintense X-Ray Pulses from the Linac Coherent Light Source Free-Electron Laser"*, Phys. Rev. Lett. 108, 245005 (2012).

[Gott77] D. Gottlieb, S.A. Orszag, "*Numerical Analysis of Spectral Methods: Theory and Applications*." CBMS Conference Series in Applied Mathematics, SIAM, 1977, p. 26

[Hau12] S. Hau-Riege, *"Photoelectron Dynamics in X-Ray Free-Electron-Laser Diffractive Imaging of Biological Samples"*, Phys. Rev. Lett. 108, 238101 (2012).

[Inou21] I. Inoue et al., *"Atomic-Scale Visualization of Ultrafast Bond Breaking in X-Ray-Excited Diamond"*, Phys. Rev. Lett. 126, 117403 (2021).

[Jenk12] T. M. Jenkins, W. R. Nelson, A. Rindi, *"Monte Carlo Transport of Electrons and Photons"*, 2012 , Springer, 978-1-4613-1059-4 (ISBN)ȷ.

[Jur16] Z. Jurek, S.-K. Son, B. Ziaja and R. Santra, *"XMDYN and XATOM: versatile simulation tools for quantitative modeling XFEL-induced dynamics of matter"*, J. Appl. Crystallogr. 49, 1048 (2016).

[Kruer88] W.L. Kruer, in *"The physics of laser plasma interactions"*, Addison Wesley Publishing Company, Inc., 1988

[Lee87] Y. T. Lee, *"A model for ionization balance and L-shell spectroscopy of non-LTE plasmas"*, J. Quant. Spectr. Rad. Tr. 38, 131 (1987).

[Levy15] A. Levy et al., *"The creation of large-volume, gradient-free warm dense matter with an X-ray free-electron laser"*, Phys. Plasm. 22, 030703 (2015).

[Lotz70] W. Lotz, *"Electron-impact ionization cross-sections for atoms up to Z=108"*, Z. Physik 232, 101-107 (1970).

[March90] R. Marchand, S. Caille, and Y. T. Lee, *"Improved screening coefficients for the hydrogenic ion model"*, J. Quant. Spectr. Rad. Tr. 43, 149 (1990).

[Medv20] N. Medvedev and I. Milov, "Electron-phonon coupling in metals at high electronic temperatures", Phys. Rev. B **102**, 064302 (2020)

[Mur98] M. S. Murillo, J. C. Weisheit, *"Dense plasmas, screened interactions and atomic ionization"*, Phys. Rep. 302, 1 (1998).

[Ng16] A. Ng et al., *"DC conductivity of two-temperature warm dense gold"*, Phys. Rev. E 94, 033213 (2016).

[Piet05] L. D. Pietanza , G. Colonna, M. Capitelli, *"Solution of the Boltzmann Equation for Electrons in Laser-Heated Metals "*,AIP Conf. Proc. 762, 1241 (2005).

[Pile11] D. Pile, et al., *"First light from SACLA."*, Nat. Photon. 5 , 456–457 (2011).

[Press03] W.H. Press et al., *"Numerical Recipes in Fortran 77"*, Cambridge University Press 2003, P.1

[Pons99] A. Pons et al., *"Evolution of Proto-Neutron Stars"*, Astrophysical J. 513, 780 (1999)

[Reth02] B. Rethfeld, A. Kaiser, M. Vicanek, G. Simon, *"Ultrafast dynamics of nonequilibrium electrons in metals under femtosecond laser irradiation"*, Phys. Rev. B 65, 214303 (2002).

[Shch13] N. S. Shcheblanov, T. E. Itina, *"Femtosecond laser interactions with dielectric materials: insights of a detailed modeling of electronic excitation and relaxation processes "*, Appl. Phys. A 110, 579 (2013).

[Sherl13] M. Sherlock, E.G. Hill and S.J. Rose, *"Kinetic simulations of the heating of solid density plasma by femtosecond laser pulses"*, HEDP 9, 38 (2013).

[Son11] S.-K. Son, L. Young, and R. Santra, *"Impact of hollow-atom formation on coherent x-ray scattering at high intensity"*, Phys. Rev. A 83, 033402 (2011).

[Son14] S.-K. Son, R. Thiele, Z. Jurek, B. Ziaja, and R. Santra, *"Quantum-Mechanical Calculation of Ionization-Potential Lowering in Dense Plasmas"*, Phys. Rev. X **4**, 031004 (2014).

[Shar66] I. P. Sharkofsky, T. W. Johnston and M. P. Bachynski, in *"The particle kinetics of plasmas"*, Addison Wesley Publishing Company Inc., 1966.

[Tachi15] T. Tachibana et al., *"Nanoplasma Formation by High Intensity Hard X rays"*, Sci. Rep. 5, 10977 (2015).

[Vink12] S.Vinko et al., *"Creation and diagnosis of a solid-density plasma with an X-ray free-electron laser"*, Nature 482, 59 (2012).

[Vink15] S. M. Vinko, *"X-ray free-electron laser studies of dense plasmas"*, J. Plasma Phys. (2015), vol. 81, 365810501]

[Weis17] H. Weise, W. Decking, *"Commissioning and first lasing of the European XFEL"*, Proc. of 38th International Free Electron Laser Conference FEL2017, Santa Fe 2017

[Zastr14] U. Zastrau et al., *"Equilibration dynamics and conductivity of warm dense hydrogen"*, Phys. Rev. E 90, 013104 (2014).

[Ziaj06] B. Ziaja, A. R. B. de Castro, E.Weckert, T. Möller, *"Modelling dynamics of samples exposed to free-electron-laser radiation with Boltzmann equations."*,
Eur. Phys. J. D 40, 465 (2006).

[Ziaj07] B. Ziaja, E.Weckert, T. Möller, *"Statistical model of radiation damage within an atomic cluster irradiated by photons from free-electron-laser."*, Laser and Particle Beams 25, 407(2007).

[Ziaj08] B. Ziaja, H. Wabnitz, E. Weckert, T. Möller, *"Atomic clusters of various sizes irradiated with short intense pulses of VUV radiation."*, Europhys. Lett. 82, 24002 (2008).

[Ziaj081] B. Ziaja, H. Wabnitz, E.Weckert, T. Möller, *"Femtosecond non-equilibrium dynamics of clusters irradiated with short intense VUV pulses."*, New J. Phys. 10, 043003 (2008).

[Ziaj09] B. Ziaja, H. Wabnitz, F. Wang, E. Weckert and T. Möller, *"Ionization and expansion dynamics of atomic clusters irradiated with short intense VUV pulses."*, Phys. Rev. Lett. 102, 205002 (2009).

[Ziaj091] B. Ziaja, T. Laarmann, H. Wabnitz, F. Wang, E. Weckert, C. Bostedt and T. Möller, *"Emission of electrons from rare gas clusters after their irradiation with intense VUV pulses of 100 nm and 32 nm wavelength."*, New J. Phys. 11, 103012 (2009).

[Ziaj11] B. Ziaja, H. N. Chapman, R. Santra, T. Laarmann, E. Weckert, C. Bostedt, T. Möller, *"Heterogeneous clusters as a model system for the study of ionization dynamics within tampered samples"*, Phys. Rev. A 84, 033201 (2011).

[Ziaj16] B. Ziaja, V. Saxena, S.-K. Son, N. Medvedev, B. Barbrel, B. Woloncewicz, M. Stransky, *"Kinetic Boltzmann approach adapted for modeling highly ionized matter created by x-ray irradiation of a solid ", Phys. Rev. E* 93, 053210 (2016).

[Ziaj21] B. Ziaja et al.,*"Tracing X-ray-induced formation of warm dense gold with Boltzmann kinetic equations"*, Eur. Phys. J. D 75, 224 (2021)